Environmentally Compatible Synthesis of Superparamagnetic Magnetite (Fe_3O_4) Nanoparticles with Prehydrolysate from Corn Stover

Chunming Zheng,[b,*] Peipei Chen,[b] Shoumin Bao,[b] Jun Xia,[b] and Xiaohong Sun [a,*]

An environmentally compatible and size-controlled method has been employed for synthesis of superparamagnetic magnetite nanoparticles with prehydrolysate from corn stover. Various characterizations involving X-ray diffraction (XRD), standard and high-resolution transmission electron microscopy (TEM and HRTEM), selected area electron diffraction (SAED), and thermogravimetric analysis (TGA) have integrally confirmed the formation of magnetite nanoparticles with homogeneous morphology and the formation mechanism of magnetite only from ferric precursor. Organic materials in the prehydrolysate act as a bifunctional agent: (1) a reducing agent to reduce ferric ions to prepare magnetite with the coexistence of ferric and ferrous ions; and (2) a coating agent to prevent particle growth and agglomeration and to promote the formation of nanoscale and superparamagnetic magnetite. The size of the magnetite nanoparticles can be easily controlled by tailoring the reducing sugar concentration, reaction time, or hydrothermal temperature.

Keywords: Magnetite; Nanoparticles; Prehydrolysate; Corn Stover; Mechanism

Contact information: a: Key Laboratory of Advanced Ceramics and Machining Technology, Ministry of Education, School of Materials Science and Engineering, Tianjin University, Tianjin 300072, People's Republic of China; b: State Key Laboratory of Hollow-fiber Membrane Materials and Membrane Processes, School of Environmental and Chemical Engineering, Tianjin Polytechnic University, Tianjin 300382, People's Republic of China;
** Corresponding authors: zhengchunming@tjpu.edu.cn; sunxh@tju.edu.cn*

INTRODUCTION

Magnetic and nano-structured iron oxides, including magnetite (Fe_3O_4), have attracted increasing attention due to their applications in many areas, such as magnetic ferrofluids, catalysts, magnetic resonance imaging (MRI), target-drug delivery, and biological species purification (Arico *et al.* 2005; Harraz 2008; Hu *et al.* 2005; Wang *et al.* 2008). With proper surface coating, these magnetic nanoparticles can be dispersed into water, forming water-based suspensions. Such a suspension can interact with an external magnetic field and be positioned to a specific area. These technological applications require that the nanoparticles are superparamagnetic with controlled size and crystallinity. The overall particle size distribution of the nanoparticles is narrow so that the particles have uniform physical and chemical properties (Sun *et al.* 2004).

Various coating materials have been employed to coat magnetic iron oxide nanoparticles, including carbon, silica, polymer, and other materials, to modify the inert surfaces of the nanoparticles and to improve their biocompatibility (Baby and Ramaprabhu, 2010; Lu *et al.* 2007; Zhang *et al.* 2008). The commonly employed approach to synthesize coated magnetic iron oxide nanoparticles requires the use and/or expensive precursors, and the reaction is often performed in an organic phase at high

temperature. The nanoparticles obtained are usually dispersible only in organic solvents, not in an aqueous phase (Lu *et al.* 2007). Thus, the development of green synthesis strategy for the coated magnetic nanostructure remains an active research field, not only for fundamental interest, but also for high efficiency and environmental conservation (Ge *et al.* 2007).

Superparamagnetic nanoparticles behave like giant paramagnetic atoms with a fast response to applied magnetic fields and with negligible remanence and coercivity. Each nanoparticle could remain as a single magnetic domain and show superparamagnetic behavior. These features make superparamagnetic nanoparticles very attractive for a broad range of biomedical applications, as they are not subject to strong magnetic interactions in dispersion, and the risk of forming agglomerates is negligible at room temperature (Jun *et al.* 2005). Iron oxide nanoparticles have received the most attention for this purpose because of their biocompatibility and stability under physiological conditions (Lin *et al.* 2010). Several robust approaches have been developed for synthesizing superparamagnetic iron oxide nanoparticles with tightly controlled size distributions to avoid the superparamagnetic–ferromagnetic transition (at a domain size of *ca*. 10 to 30 nm for Fe_3O_4). These synthesis techniques include thermal decomposition of an organometallic precursor in organic solvents, emulsion synthesis, and seed-mediated growth methods (Lu *et al.* 2007). However, the intrinsically high reaction temperature, intensive use of organic solvents, and need for complicated multistep processes are mainly responsible for the high manufacturing costs of superparamagnetic iron oxide nanoparticles, which limit their practical applications (Laurent *et al.* 2008).

Prehydrolysates of lignocelluloses are usually obtained from the pretreatment of lignocellulosic materials by acid- or alkali-based methods. Pre-hydrolysis is a necessary step in the production of bioethanol from lignocelluloses. Prehydrolysates mainly contain reducing sugars, such as glucose, xylose, and other types of saccharides. Sucrose has been used to synthesize superparamagnetic magnetite (Sun *et al.* 2009). Sun and co-workers found that reducing sugars obtained from hydrothermal treatment of sucrose played the most important role on the formation of magnetite nanoparticles in aqueous ammonium hydroxide solutions. Jeon *et al*. (2013) reported a facile synthesis method for producing magnetite particles without the use of a solvent, in which the size of the magnetite particles could be reduced to 60 nm by varying the composition of the precursor mixture containing $FeCl_3$ and palmitic acid. These authors speculated that the ferric ions were reduced by the oxidative decomposition of palmitic acid to carbon dioxide (Jeon *et al.* 2013). Compared with the methods reported, synthesis of such Fe_3O_4 nanoparticles with saccharides in the prehydrolysate from corn stover could be more environmentally compatible and cost saving because this synthesis method utilizes the saccharides present in waste prehydrolysate (Laurent *et al.* 2008). To the best of our knowledge, there have been no reports about more environmentally compatible synthesis methods for producing size-controlled superparamagnetic and coated Fe_3O_4 nanoparticles utilizing lignocellulosic prehydrolysate.

In this work, we report on the environmentally compatible and economical synthesis of superparamagnetic and coated magnetite nanoparticles utilizing corn stover hydrolysate. The materials were characterized using X-ray powder diffraction, transmission electron microscopy, thermogravimetry analysis, and magnetization measurement. Such a coating reaction method for superparamagnetic magnetite

nanoparticles provides a new method for the utilization of the hydrolysate. In addition, the detailed mechanism of the morphology-controlled magnetite formation is discussed.

EXPERIMENTAL

Materials

Corn stover was collected from Tianjin, China, and was cut into pieces 2 cm in length. The material was washed with tap water to remove contaminants and then dried at 90 °C for 8 h. The treated material was stored at -18 °C for future use. The chemical reagents used in this work (sulfuric acid, sodium hydroxide, ferric chloride, and ammonia hydroxide solution (NH_4OH, 26±1%, *w/w*)) were of analytical grade.

Preparation Methods

Dilute acid hydrolysis of corn stover

Corn stover (100 g) was treated with 1.5% (*w/w*) sulfuric acid in a screw-capped stainless steel reactor at 108 °C for 6 h. The liquid-to-solid ratio was 10:1 (*w/w*). After the reaction was complete, the reactor was cooled to below 50 °C. The wet materials were then filtered using a vacuum pump to separate the solid phase from the liquid prehydrolysate. The liquid prehydrolysate was neutralized to a pH of 10 with a sodium hydroxide solution (1 M). The above prehydrolysate was filtrated again, adjusted to a pH of 7 with a sulfuric acid solution (1 M), and then diluted to a constant volume for further use and analysis.

Synthesis of magnetite (Fe_3O_4) nanoparticles with prehydrolysate from corn stover

In a typical experiment, 2 mmol $FeCl_3$ was added to 18 mL of prehydrolysate (4.3, 7.6, or 16.3 g/L total reducing sugar) with vigorous stirring. The pH of the solution was adjusted to *ca*. 10 by the dropwise addition of 25% ammonia hydroxide solution. The obtained mixture was then transferred to a teflon-lined stainless steel autoclave (25-mL capacity) for crystallization at 120 °C for 48 h. After heating, the autoclave was allowed to cool to room temperature. The solid product was isolated from the liquid phase by centrifugation and then thoroughly washed three times with deionized water to remove residual reactants. The final product was dried overnight at 60 °C and appeared as a fine dark-black powder. In this work, the effect of the reducing sugar concentration (with 4.3, 7.6, and 16.3 g/L reducing sugar for samples (1), (2), and (3), respectively) on the particle size and the degree of magnetization of the magnetite was investigated. The effect of the hydrothermal temperature (100, 120, 150, or 180 °C) on the magnetite particle size was determined with a reducing sugar concentration of 7.6 g/L and a reaction time of 48 h. The effect of the reaction time (6, 12, 24, or 48 h) on the magnetite particle size was studied at a reducing sugar concentration of 7.6 g/L and a reaction temperature of 150 °C. It should be noted that control experiments without the addition of prehydrolysate with the above reaction procedures resulted in the formation of hematite (α-Fe_2O_3) instead of magnetite (Fe_3O_4).

Analysis and characterization of materials

The reducing sugars in the prehydrolysate were measured using the dinitro-salicylic acid (DNS) method with glucose as the standard (Hu *et al.* 2008). Carbohydrates, water extractives, and acid-insoluble lignin in the substrates were determined using

laboratory analytical procedures established by the National Renewable Energy Laboratory (Sluiter *et al.* 2010). X-ray powder diffraction (XRD) patterns of the dry samples were performed at room temperature utilizing a Rigaku D/max 2500 diffractometer with a monochromator and Cu-K_α radiation at a λ of 0.154 nm. Typically, the data were collected from 10° to 80° with a resolution of 0.2°. The average crystallite size was estimated using the Debye-Scherrer equation (Yan *et al.* 2009). Standard and high-resolution transmission electron microscopy (TEM and HRTEM), and selected area electron diffraction (SAED) measurements were performed on a Philips Tecnai F20 microscope equipped with a field emission gun at 200 kV. All samples subjected to TEM measurements were ultrasonically dispersed in alcohol and drop-cast onto copper grids. Thermogravimetric analysis (TGA) was performed using a Rigaku thermogravimetry-differential thermal analysis (TG-DTA) analyzer with a heating rate of 6 °C/min in the presence of nitrogen gas. Magnetization characterization was performed at room temperature using an LDJ 9600 VSM magnetometer.

RESULTS AND DISCUSSION

Characterization of Superparamagnetic Magnetite (Fe_3O_4) Nanoparticles

The typical chemical composition of the prehydrolysate from dilute H_2SO_4 treatment of corn stover is shown in Table 1. As shown, the main chemical composition of the prehydrolysate was monosaccharides, such as xylose, arabinose, and glucose. The content of xylose was the highest, which was approximately 75%. Glucose exhibited the lowest content of 8%. These results indicate that the xylose and arabinose were mainly hemicellulose structural units of corn stover. In addition to monosaccharide components, the prehydrolysate also contained high concentration of acetic acid and furfural. These components were also generated during the pre-hydrolysis process of corn stover.

Table 1. Chemical Composition of the Prehydrolysate from Dilute H_2SO_4 Treatment of Corn Stover

Reducing sugar (g/L)	Glucose (g/L)	Xylose (g/L)	Arabinose (g/L)	Acetic acid (g/L)	Furfural (g/L)
16.3	1.1	13.3	1.8	1.7	0.13

The crystalline structures of the iron oxide nanoparticles samples obtained from various reducing sugar concentrations of prehydrolysate were determined using the XRD patterns shown in Fig. 1(a). The patterns and relative intensities for all diffraction peaks in Fig. 1(a) matched well with those from the Joint Committee on Powder Diffraction Standards (JCPDS) card no. 19-0629 for pure magnetite. Other iron oxide or iron hydroxide phases were not observed. The broad peaks in Fig. 1(a) suggested the nanocrystallite nature of the magnetite particles (Sun *et al.* 2004). With increasing reducing sugar con-centration, there was continuous broadening of each XRD pattern peak, which was attributed to the decrease in the magnetite particle size. Using the Debye-Scherrer equation for the full width at half-maximum (fwhm) of the (311) crystal plane reflection, the average particle sizes were calculated to be 5.3, 4.5, and 3.0 nm for samples (1), (2), and (3), corresponding to reducing sugar concentrations of 4.3, 7.6, and 16.3 g/L, respectively. This observation indicated that the size control of the as-synthesized magnetite particles could be achieved by changing the reducing sugar

concentration. There was a notable decrease in the intensities of scattering lines of sample (3). This phenomenon observed was due to the less ordered crystalline structure of smaller particles. Higher pre-hydrolysate concentration will cause the "thicker coating" of an organic matter. Such kind of "thicker coating" caused disrupted crystalline growth and smaller particles of magnetite. It also caused a notable decrease in the peak intensity (Sun *et al.* 2009).

Because the XRD patterns of magnetite (Fe_3O_4) and maghemite (γ-Fe_2O_3) are very similar (Sun *et al.* 2008), Raman spectroscopy was used to distinguish the different structural phases of iron oxides. Figure 1(b) shows the Raman intensity spectrum measured for sample (3). Magnetite has a main band centered at 668 cm^{-1} (A_{1g}), whereas maghemite shows broad structures around 700, 500, and 350 cm^{-1} (Bersani *et al.* 1999). The figure shows a main feature at 668 cm^{-1}, characteristic of magnetite. No other characteristic iron oxide bands were observed. This means that the obtained iron oxide nanoparticles here are due to a pure magnetite phase without any other iron oxide phase present. The broadened Raman peaks suggest the nanocrystalline nature of Fe_3O_4, in accordance with the XRD and TEM results.

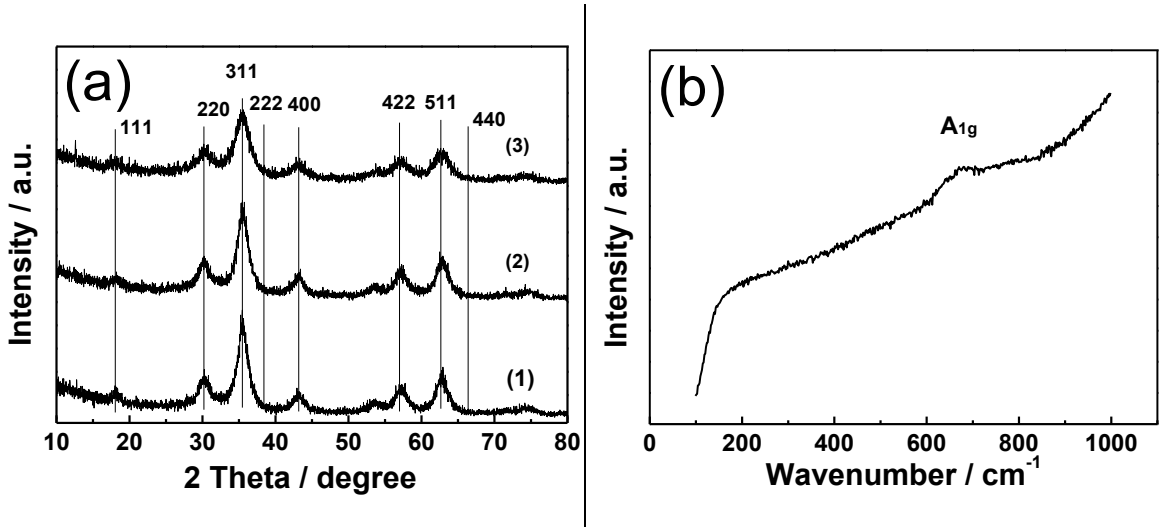

Fig. 1. Powder XRD patterns (a) of the magnetite nanoparticles at various reducing sugar concentrations (4.3, 7.6, and 16.3 g/L reducing sugar for samples (1), (2), and (3), respectively) and Raman intensity spectrum (b) of sample (3)

Figure 2 shows typical TEM, HRTEM, and SAED images of the magnetite samples obtained at various reducing sugar concentrations. TEM images in Fig. 2(a), (b), (c), and (d) showed rather uniform sizes and shapes. Based on observation of about 30 particles in the images, the average particle sizes were about 6, 5, and 3 nm, respectively, for samples (1), (2), and (3). These results were quite close to the average crystal size determined by Debye-Scherrer analysis of the X-ray diffraction. This observation indicated that all as-synthesized particles were single crystals. Clearly, the higher reducing sugar concentration led to a smaller particle size. The HRTEM image in Fig. 2(e) showed well-defined lattice planes with good crystallinity. The SAED pattern of sample (1) is shown in Fig. 2(f). This figure clearly presented well-defined rings that can be indexed to the magnetite structure (Hou *et al.* 2003). Reflections characteristic of other iron oxides were not observed.

Mechanism of Superparamagnetic Magnetite Nanoparticle Formation

To understand the function of the prehydrolysate in magnetite nanoparticle synthesis, a control experiment without the addition of prehydrolysate was performed. The XRD and TEM data of the sample obtained from the control experiment are shown in Fig. 3. The XRD pattern indicates that the control sample was hematite (α-Fe_2O_3, JCPDS card no. 33-0664). The TEM image showed that the obtained hematite was polydisperse, with a much larger particle size (*ca*. 100 nm) than to the magnetite synthesized using prehydrolysate.

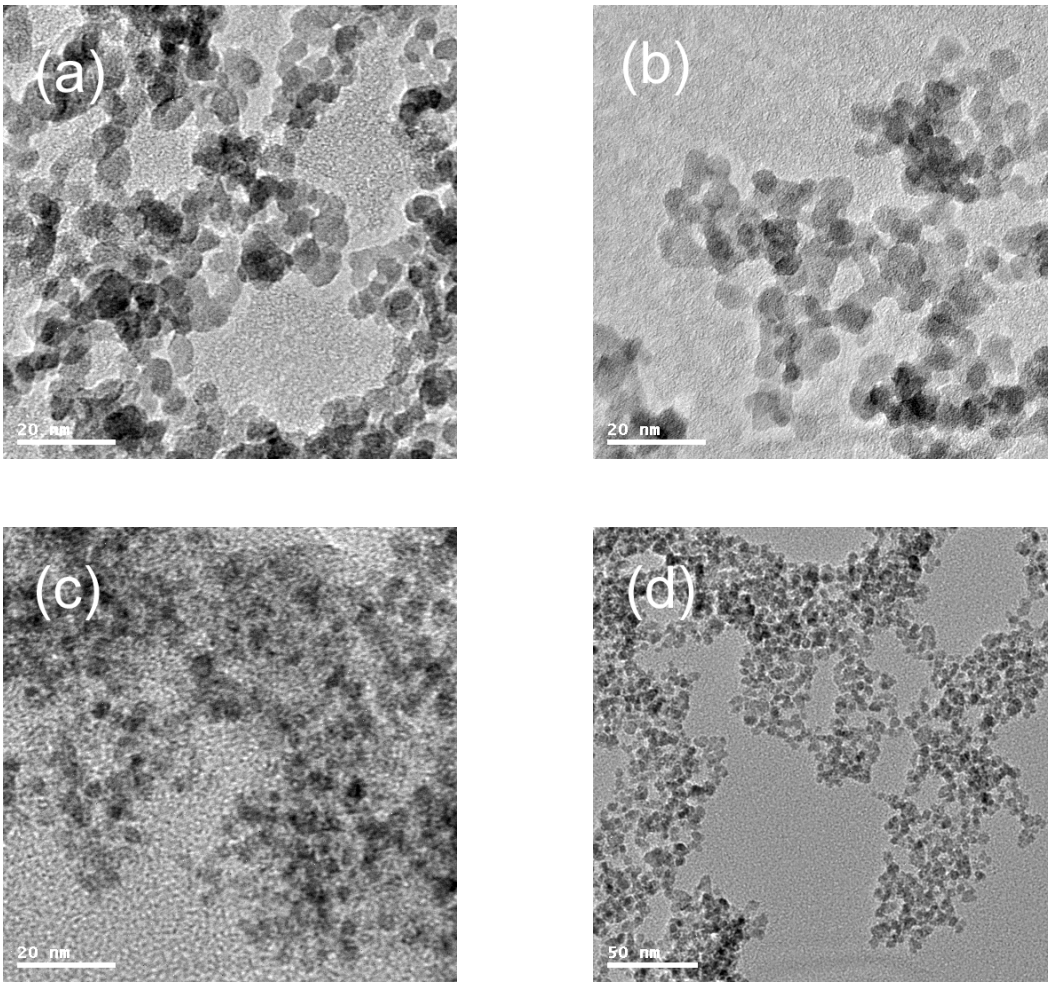

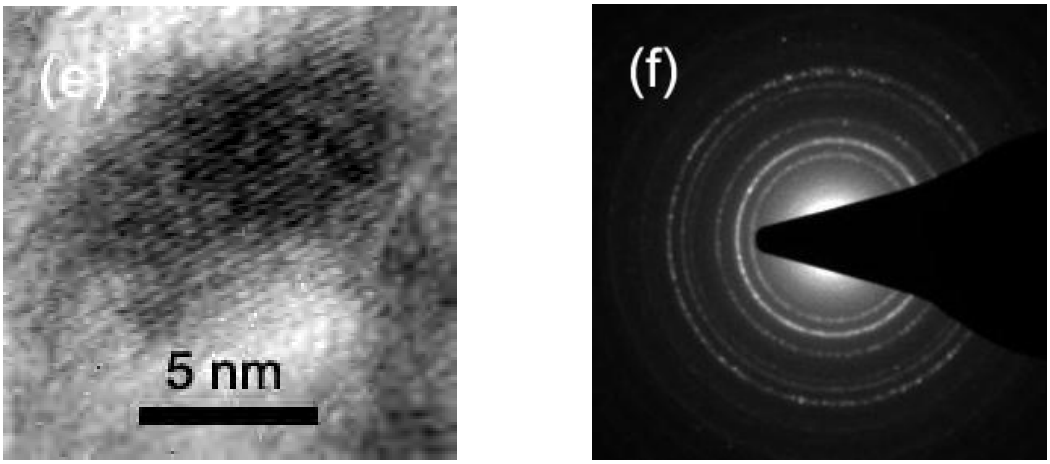

Fig. 2. TEM (a, b, c, d), HRTEM (e), and SAED (f) data for magnetite nanoparticles. Images (a), (d), (e), and (f) for sample (1); image (b) for sample (2); image (c) for sample (3)

Conventional hydrothermal synthesis usually leads to growth and aggregation of bulk particles, as shown in Fig. 3. The nucleation and subsequent growth of particles often take place in an uncontrolled manner (Cushing *et al.* 2004). It is known that mono-saccharides can chelate ferric oxide or hydroxide; they can also absorb onto certain crystal planes as a coating agent, sterically hindering subsequent crystal growth (Tang *et al.* 2005), which is similar to the role of conventional surfactants (Sun *et al.* 2008). This function leads to the nucleation and subsequent growth of the nanocrystalline phase in a controlled manner, resulting in more uniform crystalline size and morphology. The final oxidation product of reducing sugars, usually organic acids, can also chelate the magnetite particle, serving as a coating agent with the same function as glucose in the formation of magnetite nanoparticles (Wang *et al.* 2012). This means that the particle size and crystalline characteristics of magnetite nanoparticles were effectively modified by the organic components of the prehydrolysate (including xylose, glucose, other reducing sugars, and organic acids). For the obtained iron oxide nanoparticles there was a pure magnetite phase without any other iron oxide phase present. The molar ratio for the stoichiometric transformation of reactants into synthesized magnetite nanoparticles is also fixed ($Fe^{2+}/Fe^{3+} = 0.5$) during the course of the reaction.

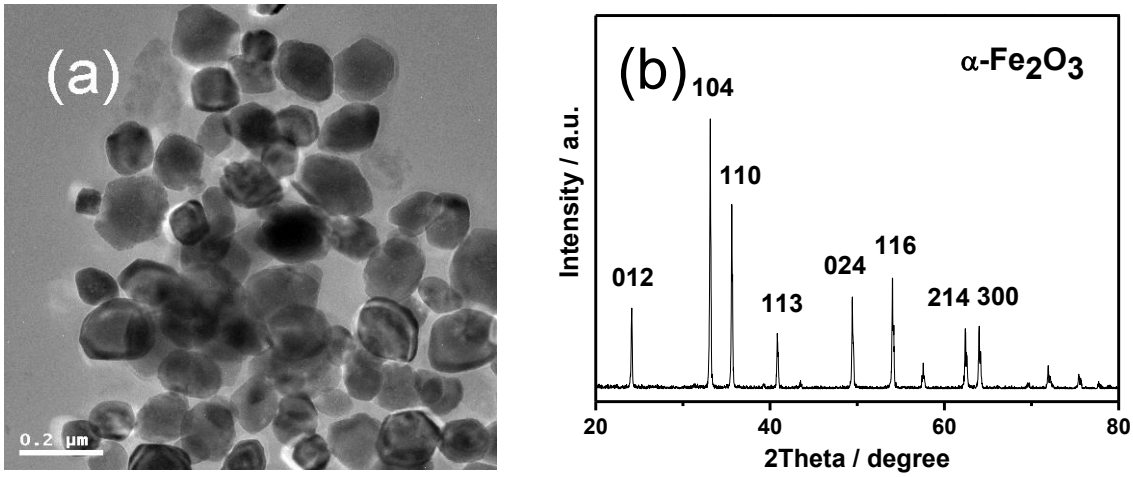

Fig. 3. TEM (a) and XRD (b) data of the sample synthesized from the control experiment without the addition of corn stover prehydrolysate

TGA measurement can also be used to identify the coating function of organic compounds. As demonstrated in Fig. 4, the TGA analysis of magnetite samples (1), (2), and (3) was performed under nitrogen atmosphere. By using this atmosphere, it was possible to minimize the mass increase caused by the oxidation of ferrous ions and only investigate the thermal decomposition of the coating agents. All the TGA curves displayed two weight loss processes. The first weight loss can be attributed to the dehydration of the magnetite, and the second one corresponded to the decomposition and subsequent evaporation of the coating agents, including reducing sugars and organic acids. In contrast to low weight loss percentages of sample (1), higher reducing sugar concentrations, which corresponded to higher weight loss percentages, favored the formation of better dispersed and smaller magnetite nanoparticles. The TGA curve of hematite (α-Fe_2O_3) indicated that the weight loss was less than 5% in relative terms. The distinct coating amount of surfactants can be expected to have a dissimilar effect on the nucleation and growth of particles. The rapid nucleation and the slow crystallization of magnetite were obtained in the presence of pre-hydrolysate, which led to the formation of uniform magnetite nanoparticles, and the particle size could be controlled easily by adjusting the pre-hydrolysate concentration.

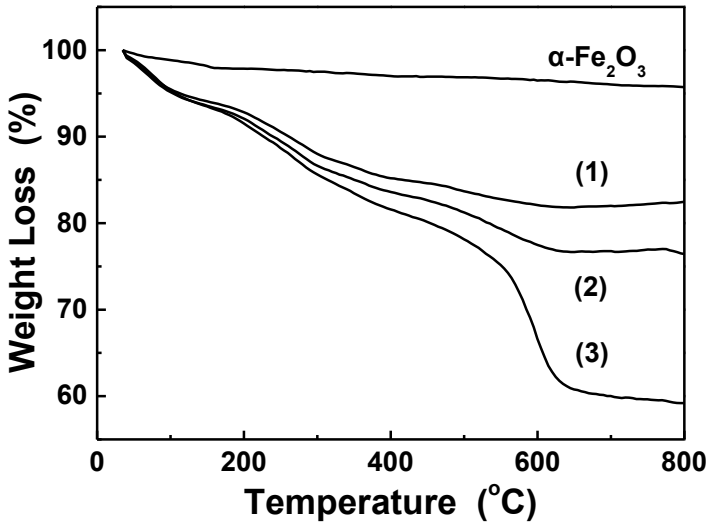

Fig. 4. TGA curves of hematite (α-Fe_2O_3) and magnetite samples synthesized at various reducing sugar concentrations (4.3, 7.6, and 16.3 g/L reducing sugar, respectively, for samples (1), (2), and (3))

Magnetization curves of the magnetite samples synthesized at various reducing sugar concentrations were measured at room temperature, as shown in Fig. 5.

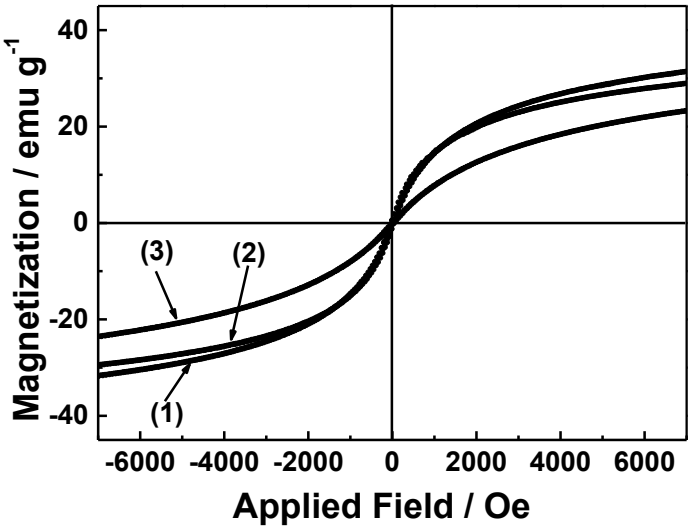

Fig. 5. Magnetization curves at room temperature of magnetite samples synthesized at various reducing sugar concentrations (4.3, 7.6, and 16.3 g/L reducing sugar, respectively, for samples (1), (2), and (3))

All the samples showed negligible coercivity and remanence, indicating that these magnetite nanoparticles were superparamagnetic at room temperature (Li *et al.* 2005). This is in accordance with the theory that superparamagnetic behavior is often observed at room temperature for magnetite particles with particle sizes smaller than 20 nm (Daou

et al. 2006). The saturation magnetizations (*Ms*) of the samples (1), (2), and (3) were 31.65, 29.60, and 23.44 emu g^{-1}, respectively, at a 7-kOe (577-kA/m) applied magnetic field strength. The differences in the saturation magnetizations for the magnetite samples can be attributed to the decrease in the particle size and the reduction of the coating concentration (Bai *et al.* 2009; Goya *et al.* 2003). A lower saturation magnetization of all the samples compared to that of bulk magnetite (92 emu g^{-1}) (Bai *et al.* 2009) is often observed with nanoparticles. This is mainly due to the existence of organic coating agents (Kim *et al.* 2003).

Size Control of Superparamagnetic Magnetite Nanoparticles using Reaction Temperature and Reaction Time

The above results indicated that size control of superparamagnetic magnetite could be achieved by varying the reducing sugar concentration. At the same time, the particle size and the crystallinity of magnetite could also be controlled by adjusting the reaction time (*t*) and the hydrothermal temperature (*T*) (Li *et al.* 2005). The effect of reaction time is shown in Fig. 6. Increasing the reaction time resulted in a continuous narrowing of each XRD pattern peak, which can be attributed to increasing particle size and crystallinity. Using the Debye-Scherrer equation for the full width at half-maximum (fwhm) of the (311) reflection, the average particle sizes were calculated to be 7.6, 9.5, 10.7, and 13.5 nm for reaction times of 6, 12, 24, and 48 h, respectively.

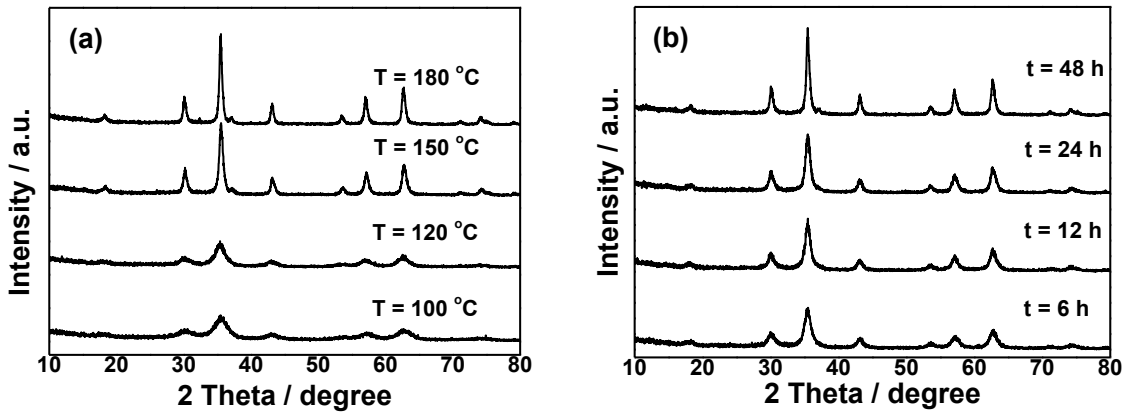

Fig. 6. XRD patterns of magnetite synthesized at different hydrothermal temperatures (a) and reaction times (b)

The hydrothermal temperature had a similar effect on the particle size and crystallinity. Using the Debye-Scherrer equation, the average particle sizes of the synthesized magnetite with increasing temperature were calculated to be 3.6, 4.8, 12.9, and 19.9 nm for temperatures of 100, 120, 150, and 180 °C, respectively. Hence, it is easy to control the particle size and the crystallinity of the synthesized magnetite using the prehydrolysate-assisted hydrothermal method described in this study. The reaction temperature and reaction time dependence of the size distribution followed the same trend and could be explained in terms of Ostwald ripening of the magnetite nanoparticles. The nucleation process was almost the same for the magnetite nanoparticles, while in the growth process the temperature and time were changed. The critical nuclei size changed since the solubility and the saturation ratio in the liquid are dependent on the temperature. At higher temperatures, the solubility and saturation ratio were raised. The nuclei smaller

than the critical nuclei size will dissolve and redeposit onto larger crystals to achieve their growth. In this process the surface energy decreases (driving force) while the volume energy increases. Therefore, the final size will be obtained at the minimized total energy in the system (Guo *et al.* 2009). Therefore, the minimum size of the particles increases with the reaction temperature and reaction time for individual samples, as observed in the XRD and TEM results.

CONCLUSIONS

1. Superparamagnetic magnetite nanoparticles were successfully synthesized using an environmentally compatible corn stover prehydrolysate-assisted hydrothermal method.
2. The particle size and crystalline characteristics of the synthesized magnetite nano-particles were effectively modified by the organic compounds in the prehydrolysate. The particle size and crystallinity of the magnetite could be controlled easily by adjusting the reducing sugar concentration of the prehydrolysate.
3. The mechanism of superparamagnetic magnetite nanoparticles was studied. Organic compounds in the prehydrolysate act as a bifunctional agent: (1) as a reducing agent to reduce ferric ions for the formation of magnetite; and (2) as a coating agent and crystal growth modifier to control the particle size with superparamagnetic property.
4. The saturation magnetization (*M*s) of the obtained magnetite is directly related to the particle size. The particle size and crystallinity of the magnetite could also be controlled easily by adjusting the reaction time and/or the hydrothermal temperature.

ACKNOWLEDGMENTS

The authors are grateful for the support of: the National Natural Science Foundation of China, NSFC (21101113, 51202159, 51208357, and 51372166); the Fund for the Doctoral Program of Higher Education, the Ministry of Education of China (20120032120017); the Key Project of the Chinese Ministry of Education (211066); the General Program of the Municipal Natural Science Foundation of Tianjin (13JCYBJC16900 and 13JCQNJC08200); the Yunnan Province-University Cooperation Foundation (2011IB002); and the Beiyang Scholar Plan for Excellent Young Teachers of Tianjin University.

REFERENCES CITED

Arico, A. S., Bruce, P., Scrosati, B., Tarascon, J. M., and Van Schalkwijk, W. (2005). "Nanostructured materials for advanced energy conversion and storage devices," *Nat. Mater.* 4(5), 366-377.

Baby, T. T., and Ramaprabhu, S. (2010). "SiO_2 coated Fe_3O_4 magnetic nanoparticle dispersed multiwalled carbon nanotubes based amperometric glucose biosensor," *Talanta* 80(5), 2016-2022.

Bai, W., Meng, X. J., Zhu, X., Jing, C. B., Gao, C., and Chu, J. H. (2009). "Shape-tuned synthesis of dispersed magnetite submicro particles with good magnetic properties," *Physica E* 42(2), 141-145.

Bersani, D., Lottici, P. P., and Montenero, A. (1999). "Micro-Raman investigation of iron oxide films and powders produced by sol-gel syntheses," *J. Raman Spectrosc.* 30(5), 355-360.

Cushing, B. L., Kolesnichenko, V. L., and O'Connor, C. J. (2004). "Recent advances in the liquid-phase syntheses of inorganic nanoparticles," *Chem. Rev.* 104(9), 3893-3946.

Daou, T. J., Pourroy, G., Begin-Colin, S., Greneche, J. M., Ulhaq-Bouillet, C., Legare, P., Bernhardt, P., Leuvrey, C., and Rogez, G. (2006). "Hydrothermal synthesis of monodisperse magnetite nanoparticles," *Chem. Mater.* 18(18), 4399-4404.

Ge, J. P., Hu, Y. X., Biasini, M., Dong, C. L., Guo, J. H., Beyermann, W. P., and Yin, Y. D. (2007). "One-step synthesis of highly water-soluble magnetite colloidal nanocrystals," *Chem. Eur. J.* 13(25), 7153-7161.

Goya, G. F., Berquo, T. S., Fonseca, F. C., and Morales, M. P. (2003). "Static and dynamic magnetic properties of spherical magnetite nanoparticles," *J. Appl. Phys.* 94(5), 3520-3528.

Guo, S. J., Li D., Zhang L. X., Li J., Wang E. K. (2009). "Monodisperse mesoporous superparamagnetic single-crystal magnetite nanoparticles for drug delivery," *Biomaterials* 30(10), 1881-1889.

Harraz, F. A. (2008). "Polyethylene glycol-assisted hydrothermal growth of magnetite nanowires: Synthesis and magnetic properties," *Physica E* 40(10), 3131-3136.

Hou, Y. L., Yu, J. F., and Gao, S. (2003). "Solvothermal reduction synthesis and characterization of superparamagnetic magnetite nanoparticles," *J. Mater. Chem.* 13(8), 1983-1987.

Hu, A. G., Yee, G. T., and Lin, W. B. (2005). "Magnetically recoverable chiral catalysts immobilized on magnetite nanoparticles for asymmetric hydrogenation of aromatic ketones," *J. Am. Chem. Soc.* 127(36), 12486-12487.

Hu, R. F., Lin, L., Liu, T. J., Ouyang, P. K., He, B. H., and Liu, S. J. (2008). "Reducing sugar content in hemicellulose hydrolysate by DNS method: A revisit," *J. Biobased Mater. Bio.* 2(2), 156-161.

Jeon, Y., Thangadurai, D. T., Piao, L., and Yoon, S. (2013). "A facile one-step method to prepare size controlled Fe_3O_4 submicro/nanoparticles," *Mater. Lett.* 96, 27-30.

Jun, Y. W., Huh, Y. M., Choi, J. S., Lee, J. H., Song, H. T., Kim, S., Yoon, S., Kim, K. S., Shin, J. S., Suh, J. S., and Cheon, J. (2005). "Nanoscale size effect of magnetic nanocrystals and their utilization for cancer diagnosis via magnetic resonance imaging," *J. Am. Chem. Soc.* 127(16), 5732-5733.

Kim, D. K., Mikhaylova, M., Zhang, Y., and Muhammed, M. (2003). "Protective coating of superparamagnetic iron oxide nanoparticles," *Chem. Mater.* 15(8), 1617-1627.

Laurent, S., Forge, D., Port, M., Roch, A., Robic, C., Elst, L. V., and Muller, R. N. (2008). "Magnetic iron oxide nanoparticles: Synthesis, stabilization, vectorization, physicochemical characterizations, and biological applications," *Chem. Rev.* 108(6), 2064-2110.

Li, Z., Sun, Q., and Gao, M. Y. (2005). "Preparation of water-soluble magnetite nanocrystals from hydrated ferric salts in 2-pyrrolidone: Mechanism leading to Fe_3O_4," *Angew. Chem. Int. Ed.* 44(1), 123-126.

Lin, M. M., Kim, H. H., Kim, H., Dobson, J., and Kim, D. K. (2010). "Surface activation and targeting strategies of superparamagnetic iron oxide nanoparticles in cancer-oriented diagnosis and therapy," *Nanomedicine* 5(1), 109-133.

Lu, A. H., Salabas, E. L.,and Schuth, F. (2007). "Magnetic nanoparticles: Synthesis, protection, functionalization, and application," *Angew. Chem. Int. Ed.* 46(8), 1222-1244.

Sluiter, J. B., Ruiz, R. O., Scarlata, C. J., Sluiter, A. D., and Templeton, D. W. (2010). "Compositional analysis of lignocellulosic feedstocks. 1. Review and description of methods," *J. Agric. Food Chem.* 58(16), 9043-9053.

Sun, S. H., Zeng, H., Robinson, D. B., Raoux, S., Rice, P. M., Wang, S. X., and Li, G. X. (2004). "Monodisperse MFe_2O_4 (M = Fe, Co, Mn) nanoparticles," *J. Am. Chem. Soc.* 126(1), 273-279.

Sun, X. H., Zheng, C. M., Zhang, F. X., Li, L. D., Yang, Y. L., Wu, G. J., and Guan, N. J. (2008). "Beta-cyclodextrin-assisted synthesis of superparamagnetic magnetite nanoparticles from a single Fe(III) precursor," *J. Phys. Chem. C* 112(44), 17148-17155.

Sun, X. H., Zheng, C. M., Zhang, F. X., Yang, Y. L., Wu, G. J., Yu, A. M., and Guan, N. J. (2009). "Size-controlled synthesis of magnetite (Fe_3O_4) nanoparticles coated with glucose and gluconic acid from a single Fe(III) precursor by a sucrose bifunctional hydrothermal method," *J. Phys. Chem. C* 113(36), 16002-16008.

Tang, J., Redl, F., Zhu, Y. M., Siegrist, T., Brus, L. E., and Steigerwald, M. L. (2005). "An organometallic synthesis of TiO_2 nanoparticles," *Nano Lett.* 5(3), 543-548.

Wang, P., Shi, Q. H., Liang, H. J., Steuerman, D. W., Stucky, G. D., and Keller, A. A. (2008). "Enhanced environmental mobility of carbon nanotubes in the presence of humic acid and their removal from aqueous solution," *Small* 4(12), 2166-2170.

Wang, X., Xu, Y., Fan, L., Yong, Q., and Yu, S. (2012). "Simultaneous separation and quantitative determination of monosacccharides, uronic acids, and aldonic acids by high performance anion-exchange chromatography coupled with pulsed amperometric detection in corn stover prehydrolysates," *BioResources* 7(4), 4614-4625.

Yan, H., Zhang, J. C., You, C. X., Song, Z. W., Yu, B. W., and Shen, Y. (2009). "Influences of different synthesis conditions on properties of Fe_3O_4 nanoparticles," *Mater. Chem. Phys.* 113(1), 46-52.

Zhang, W. M., Wu, X. L., Hu, J. S., Guo, Y. G., and Wan, L. J. (2008). "Carbon coated Fe_3O_4 nanospindles as a superior anode material for lithium-ion batteries," *Adv. Funct. Mater.* 18(24), 3941-3946.

Article submitted: August 14, 2013; Peer review completed: October 18, 2013; Revised version received and accepted: November 27, 2013; Published: December 3, 2013.